Formation of Copper–Chromium Sulfide Spinel and Thermal Decomposition Reactions in CuS–Cr₂S₃ Crystalline Mixtures

El-H. M. Diefallah,*·[1] A. Y. Obaid,* A. A. Samarkandy,* M. M. Abel Badei,† and A. A. El-Bellihi†

*Department of Chemistry, Faculty of Science, King Abdulaziz University, Jeddah, Saudi Arabia; and
†Department of Chemistry, Faculty of Science, Benha, Egypt

Differential thermal analysis–thermogravimetry (DTA–TG), X ray diffraction (XRD), and scanning electron microscopy (SEM) techniques were used to study the formation of $CuCr_2S_4$ spinel and the thermal decomposition reactions in crystalline mixtures of copper and chromium sulfides. The copper–chromium sulfide spinel was characterized by XRD and SEM and the kinetics of formation was followed in the temperature range 200–300°C by a titrimetric method. Kinetic analysis in view of various solid-state reaction models showed that the reaction is best described by the diffusion models with an average activation energy 24.6 ± 1.6 kJ/mol. © 1995 Academic Press, Inc.

INTRODUCTION

Oxide and sulfide spinels represent a large class of inorganic materials which possess many useful properties not found in the more limited binary oxides and sulfides. Sulfide spinels show a much greater variation in their electrical and magnetic properties than the corresponding oxide spinels. A number of sulfide spinels with composition AB_2S_4, where A and B are di- and trivalent transition metals, have been reported in the literature (1–3). Thio-chromites of the type ACr_2S_4 are particularly attractive because they are all probably ordered in the normal spinel structure (4), i.e., only divalent ions on the tetrahedral sites and only trivalent ions on the octahedral sites.

A limited number of studies has been carried out on the kinetics and mechanisms of spinel formation in the solid state (5–9). Carter (5) and Rossi and Fulrath (6) studied the kinetics and mechanism of the reaction between MgO and Al_2O_3 to form $MgAl_2O_4$ (spinel); Branson (7) studied the kinetics of the reaction between ZnO and Al_2O_3 using X ray diffraction and found that the activation energy of the $ZnAl_2O_4$ formation reaction is 226.8 kJ/mol according to the diffusion-controlled reaction and 120.1 kJ/mol according to the phase boundary reaction. Diefallah et al. (8) studied the kinetics of $MgFe_2O_4$ formation reaction in powdered mixtures of MgO and Fe_2O_3 with different mole ratios and the results were discussed in terms of Jander's diffusion equation. El-Bellihi et al. (9) studied the kinetics of copper ferrite and copper chromite formation and found that the results are best described by Jander's and Ginstling–Brounshtein diffusion equations. However, the kinetics of formation of sulfide spinels have not been studied in any detail. In the present work, the phase and chemical transformation reactions and the kinetics of formation of copper–chromium sulfide spinels in CuS–Cr₂S₃ crystalline mixtures are discussed.

EXPERIMENTAL

Samples of copper sulfide, chromium sulfide, or their mixtures were prepared by direct precipitation or coprecipitation, using sodium sulfide solution added dropwise to a solution containing the calculated amount of the AnalaR salt chlorides. The fine precipitates were filtered, washed several times with distilled water until impurity-ion free, and then dried at 90°C to a constant weight. The resultant mixtures were calcined at the desired temperature for different durations of time in air and then cooled to room temperature and analyzed.

X ray diffraction patterns for CuS, Cr_2S_3, and their calcined mixtures (1 : 1 mole ratio) were performed with the aid of Shimadzu X ray diffraction unit using a Cu target and an Ni filter. Simultaneous DTA–TG behavior of the CuS–Cr₂S₃ system was investigated using a Shimadzu Model 30 thermal analyzer. Experiments were carried out against α-Al_2O_3 as a reference, at constant heating rate of 20°C/min. Scanning EM photographs of samples were taken using a Jeol JSM-35C scanning electron microscope.

The rate of spinel formation reaction was followed under isothermal conditions using a titrimetric method which depends on selective dissolution of the spinel in aqueous ammonia solution, leaving behind the unreacted CuS and Cr_2S_3. Samples, accurately about 100 mg of the sulfide mixture containing a known amount of CuS, were calcined

[1] To whom correspondence should be addressed.

for different durations at 200, 250, and 270°C. The calcined sample was rapidly cooled from the calcination temperature to room temperature and shaken vigorously with 30 ml of 1 : 4 ammonia–water solution for about 3 hr. The $CuCr_2S_4$ spinel dissolves, leaving behind the unreacted CuS and Cr_2S_3. The solution was filtered and diluted with distilled water, and then 10 ml of ammonia buffer solution and 1 g murexide indicator were added to the filterate. The mixture was titrated with 1.00×10^{-2} M versene solution till a blue-violet color appeared, marking the equivalence point. Alternatively, the product $CuCr_2S_4$ spinel was dissolved by shaking the calcined sample with 1.0 M HCl. The Cu(II) in solution was then determined iodometrically by adding a few grams of KI and then titrating with standard sodium thiosulfate solution. Both methods gave concordant results within experimental errors. From the original weight of CuS in the calcined sample and the weight of reacted CuS, the fractional reaction (α) is obtained.

RESULTS AND DISCUSSION

Figures 1–3 show DTA–TG curves in air obtained for precipitated samples of CuS, Cr_2S_3, and the CuS–Cr_2S_3 (1 : 1 mole ratio) mixture, respectively. The DTA curve of copper sulfide (Fig. 1) shows an endothermic peak at about 100°C, accompanied by a weight loss of about 8.5% due to removal of the loosely bound surface water molecules. A small endothermic peak at 220°C due to removal of coordinated water molecules, accompanied by a weight loss in TG, is followed at about 280°C by a large and sharp
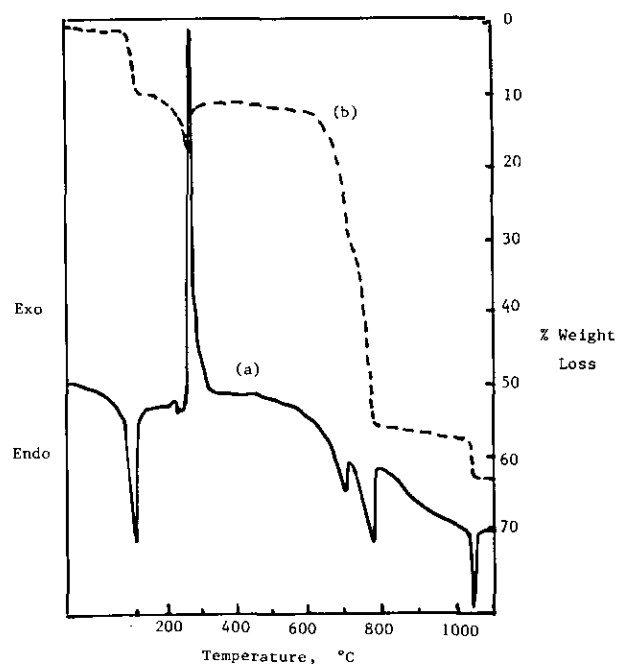

FIG. 2.   DTA (a) and TG (b) curves of $Cr_2S_3 \cdot xH_2O$.

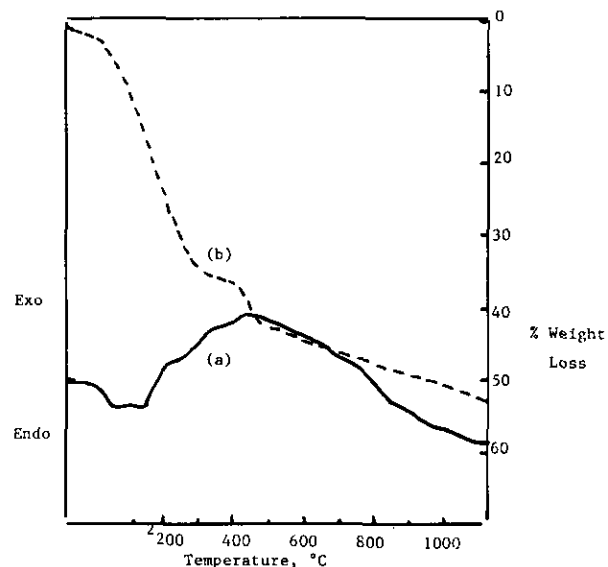exothermic peak accompanied with about 6% increase in weight due to partial oxidation of CuS to $CuSO_4$ (12). DTA–TG study of pentlandite (a sulfide mineral having the stoichiometry $Ni_{4.90}Fe_{4.45}S_8$, as determined by electron probe microanalysis (13)) in air showed a 3% mass gain at about 590°C due to partial oxidation of the nickel and iron sulfides and the formation of iron and nickel sulfates (13). Figure 1 showed also two endothermic peaks around 710 and 775°C due to decomposition of the remaining CuS to CuO and of $CuSO_4$ to CuO, respectively. An endother-
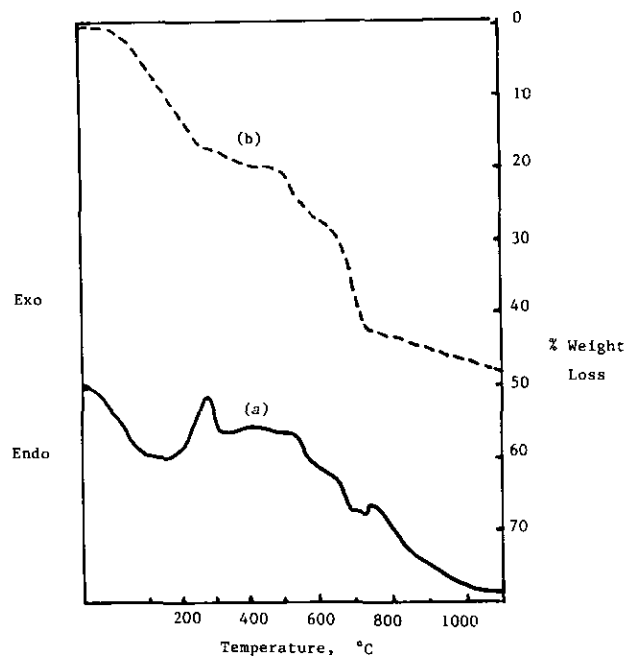

FIG. 1.   DTA (a) and TG (b) curves of CuS · xH_2O.

FIG. 3.   DTA (a) and TG (b) curves of CuS–Cr_2S_3 coprecipitated mixture (1 : 1 mole ratio).
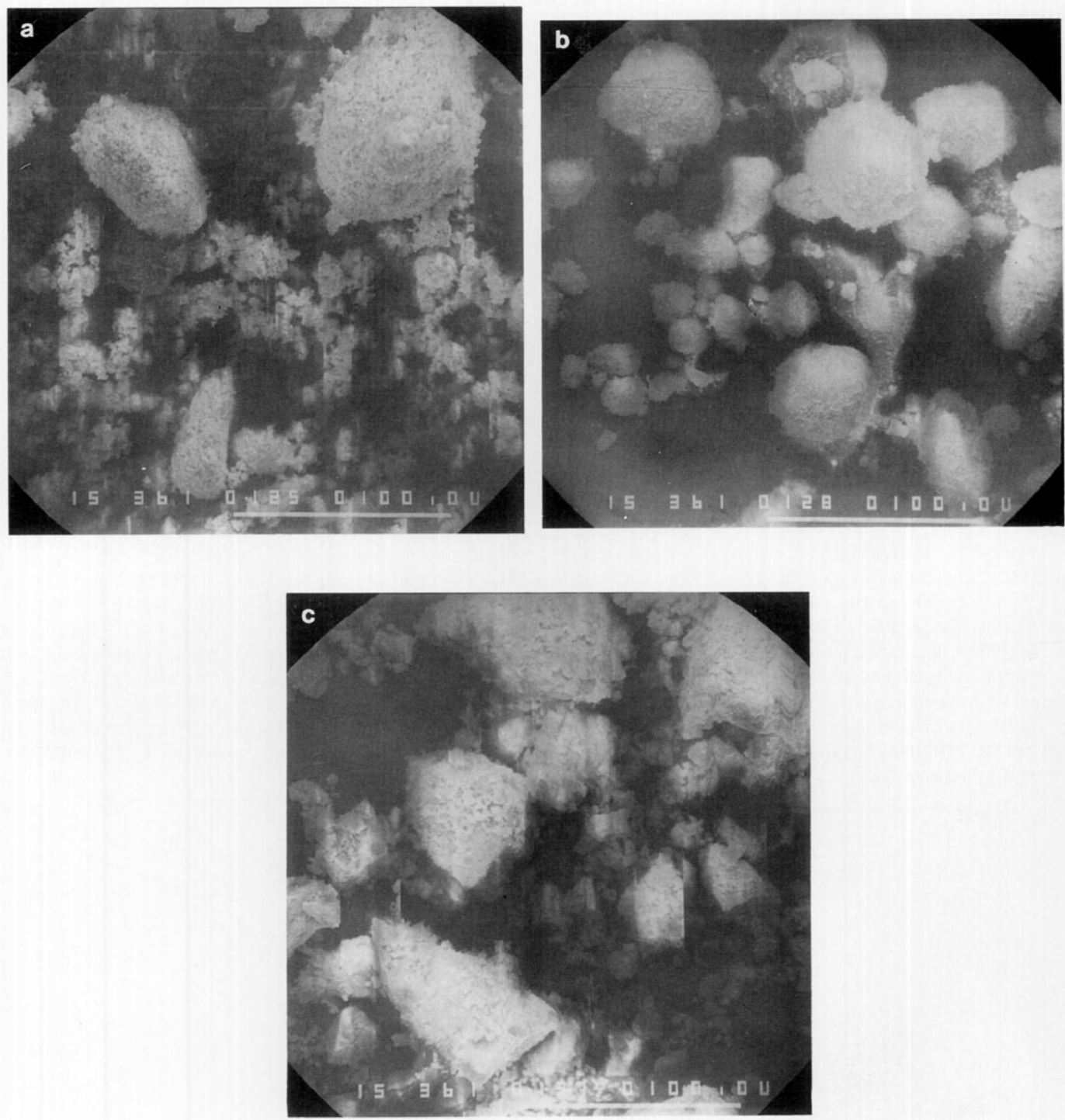
FIG. 4.   SEM micrographs of samples dried at 90°C of (a) CuS, (b) Cr_2S_3, and (c) $CuS-Cr_2S_3$ (1 : 1 mole ratio).

mic peak located at 1050°C is due to the decomposition of CuO to Cu_2O accompanied with loss in weight by about 5.0% (calculated value 4.5%).

DTA–TG curves of precipitated chromium sulfide (Fig. 2) showed a broad endothermic peak at 100°C due to elimination of loosely bound water molecules accompanied with loss in weight by about 34%. This is followed

by a broad exothermic peak around 450°C due to oxidation of Cr_2S_3 to Cr_2O_3.

Figure 3 shows DTA–TG study of the coprecipitated $CuS-Cr_2S_3$ (1 : 1 mole ratio) mixture. The endothermic peak at 1050°C in the DTA–TG curves of copper sulfide (Fig. 1), due to decomposition of CuO to Cu_2O has disappeared in the DTA–TG curves of the mixture. The rapid
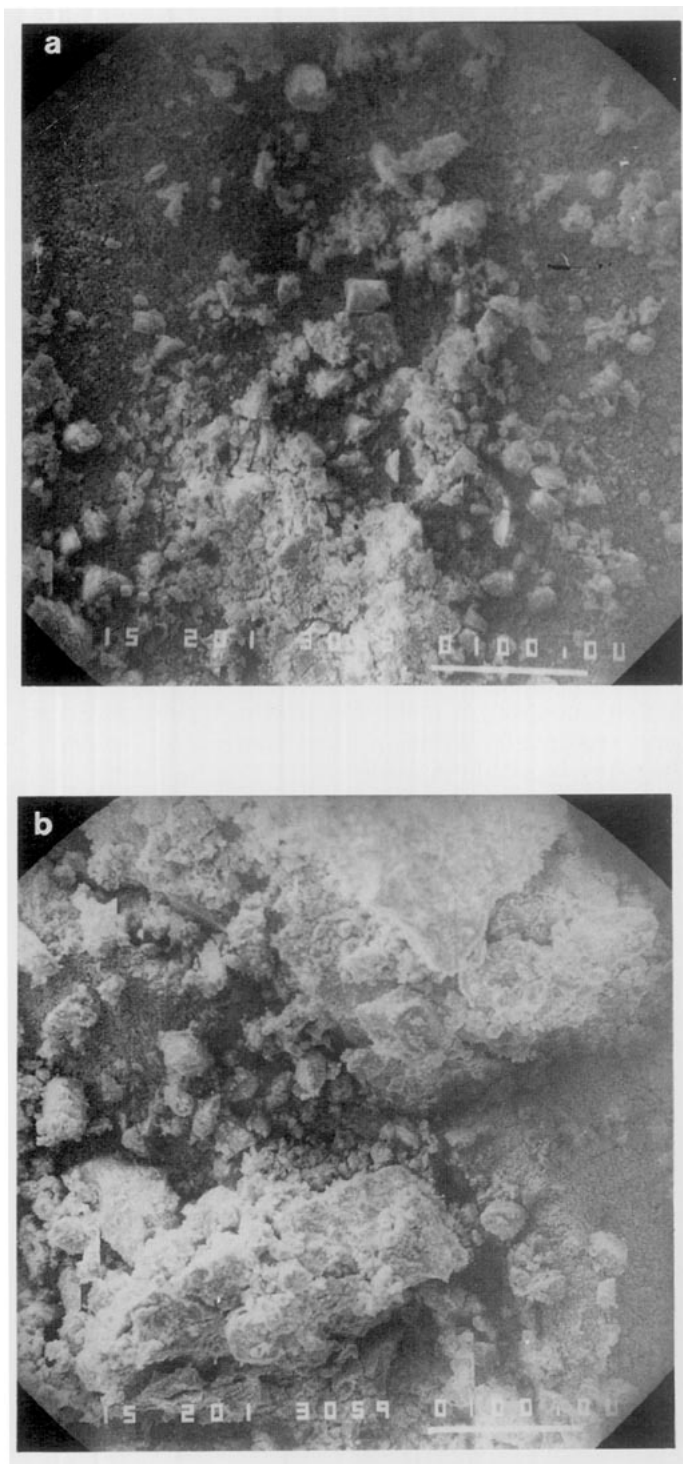
effects. However, the disappearance of the peak at 1050°C (Fig. 1), in the DTA–TG curves of the mixture (Fig. 3), indicates that CuO reacted with Cr_2O_3 to give copper chromite oxide spinel (9). DTA–TG curves in N_2 atmosphere for samples of the (Cu–Cr)S system dried at 90°C showed that the oxidation steps discussed above are hindered.

The formation of $CuCr_2S_4$ spinel in the $CuS–Cr_2S_3$ mixture was shown by X ray diffraction pattern experiments for samples calcined at 200–300°C. Above 300°C, X ray diffraction lines characteristic of $CuSO_4$ appeared. The intensity of lines due to $CuSO_4$ increases as the calcination temperature increases for samples calcined above 300°C. These results show that the study of the sulfide spinel formation reaction must be limited to temperatures below 300°C.

Samples of pure and mixed sulfides were examined by scanning electron microscopy, as prepared during their thermal decompositions. SEM micrographs of samples of pure CuS and Cr_2S_3 and (Cu–Cr) sulfide mixture (1 : 1 mole ratio), dried at 90°C are shown in Fig. 4. The original reactants consisted approximately of spherical particles (grain size about 20–60 μm) which reveal the participation of liquid water (14). The micrograph of a sample of the (Cu–Cr) sulfide calcined at 200°C for 5 hr is shown in Fig. 5a. There is a remarkable change in both the size and morphology of the particles, and the sulfide spinel appears as small cubic crystallites (grain size about 10–20 μm) which look coherent with sharp edges. Figure 5b shows the micrograph of a sample of (Cu–Cr) sulfide mixture

FIG. 5. SEM micrographs of calcined samples of $CuS–Cr_2S_3$ (1 : 1 mole ratio) calcined for 5 hr at (a) 200°C and (b) 350°C.

water loss at about 100°C found for the copper sulfide is not equally evident in the coprecipitate. The DTA curve of the mixture did not show observable thermal effects due to formation of sulfide spinel during the course of heating the mixture. This indicates that the spinel formation reaction is not accompanied by significant thermal
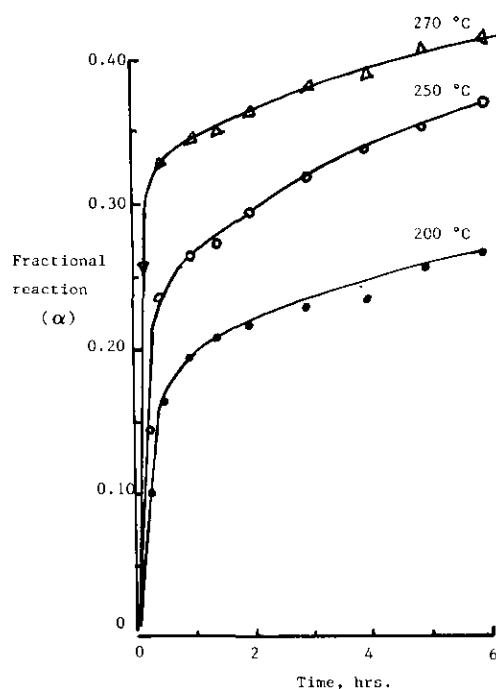

FIG. 6. Plots of fractional reaction (α) versus time (t) for the formation of $CuCr_2S_4$ spinel.

calcined at 350°C for 5 hr. At this temperature the particles grow in size and lose most of their cubic shape due to significant partial oxidation of the sulfides.

The kinetics of the $CuCrS_4$ formation reaction was studied under isothermal conditions in the temperature range 200–300°C. Kinetic analysis of isothermal data obtained for the fractional reaction (α) formed as a function of time (t) and shown in Fig. 6 were analyzed in view of the various solid-state kinetic equation models (11, 15). Under isothermal conditions the α–t curves are expressed in the form $g(\alpha) = kt$, where k is the rate constant and the function $g(\alpha)$ depends on the mechanism controlling the reaction and on the size and shape of the reacting particles. For the phase boundary-controlled reactions, we have the contracting area or R_2 model, $g(\alpha) = 1 - (1 - \alpha)^{1/2}$ and the contracting sphere or R_3 model, $g(\alpha) = 1 - (1 - \alpha)^{1/3}$. For the diffusion-controlled reactions, analyses were performed with reference to a one-dimensional diffusion process governed by a parabolic law, D_1 function, $g(\alpha) = \alpha^2$; a two-dimensional diffusion-controlled process in a cylinder, D_2 function, $g(\alpha) = (1 - \alpha) \ln(1 - \alpha) + \alpha$; Jander's equation for a diffusion-controlled reaction in a sphere, D_3 function, $g(\alpha) = [1 - (1 - \alpha)^{1/3}]^2$; the Ginstling–Brounshtein equation for a diffusion-controlled reaction starting on the exterior of a spherical particle, D_4 function, $g(\alpha) = (1 - (2\alpha/3)) - (1 - \alpha)^{2/3}$; the Zhuravlev–Losokhim–Tempel'man diffusion equation, D_5 function, $g(\alpha) = [(1/(1 - \alpha)^{1/3}) - 1]^2$; and the Kroger–Ziegler diffusion equation, D_6 function, $k \ln t = [1 - (1 - \alpha)^{1/3}]^2$. If the solid-state reaction is controlled by nucleation followed by growth, then in this case, we may have the Mampel unimolecular law, where the rate-determining step is the nucleation process described by the F_1 function, $g(\alpha) = -\ln(1 - \alpha)$; the Avrami equation for initial random nucleation followed by overlapping growth in two-dimensions, A_2 function, $g(\alpha) = [-\ln(1 - \alpha)]^{1/2}$; the Erofeev equation for initial random nucleation followed by overlapping growth in three dimensions, A_3 function, $g(\alpha) = [-\ln(1 - \alpha)]^{1/3}$; and the Prout–Thomkins equation for branching nuclei, A_1 function, $g(\alpha) = \ln[\alpha/(1 - \alpha)]$.

Table 1 shows that the best fit of the kinetic data of the reaction was obtained with the diffusion-controlled models: D_2, D_3, D_4, and D_5 equations. The other solid-state reaction rate equations: the phase boundary-controlled reaction models, the first-order kinetics, and the Avrami–Erofeev random nucleation models gave less satisfactory fits. The activation energy for the $CuCr_2S_4$ spinel formation reaction was calculated by regression analysis according to the two-dimensional diffusion-controlled, the three-dimensional diffusion-controlled, Jander's and Ginstling-Brounshtein equations, and the three models, giving an average activation energy of 24.6 ± 1.6 kJ mole^{-1}. This value is much less than the value obtained

TABLE 1

Comparison of Fit of Various Kinetic Models to the α/t Curves for $CuCr_2S_4$ Spinal Formation Reaction

Function symbol	Correlation coefficient, r		
	(200°C)	(250°C)	(270°C)
R_2	0.9662	0.9842	0.9885
R_3	0.9670	0.9849	0.9888
D_1	0.9786	0.9914	0.9912
D_2	0.9822	0.9929	0.9922
D_3	0.9814	0.9943	0.9932
D_4	0.9805	0.9934	0.9926
D_5	0.9837	0.9966	0.9950
D_6	0.9734	0.9724	0.9734
F_1	0.9684	0.9865	0.9896
A_1	0.9485	0.9745	0.9851
A_2	0.9581	0.9798	0.9868
A_3	0.9541	0.9773	0.9858

for the activation energy of formation of the $CuCr_2O_4$ spinel (97.6 ± 3.5 kJ mole^{-1}). The sulfide spinel formation reaction occurs at a much lower temperature and the energy required for diffusion is less than that for the oxide spinel. It is possible that since one is dealing with a sequence of chemical reactions involving exo- and endothermic steps, the resultant activation energy, having a composite value, is probably controlled by a diffusion step.

ACKNOWLEDGMENT

REFERENCES

1. H. Han and H. Harder, Z. Anorg. Allgem. Chem. **288**, 257 (1956).
2. G. Blasse and D. J. Schipper, J. Inorg. Nucl. Chem. **26**, 1467 (1964).
3. F. K. Lotgering, Solid State Commun. **2**, 55 (1964).
4. N. M. Kovtum, V. K. Prokopenko, and A. Ashamyakov, Solid State Commun. **26**, 877 (1978).
5. R. E. Carter, J. Chem. Phys. **34**, 2010 (1961); J. Am. Ceram. Soc. **44**, 116 (1961).
6. R. C. Rossi and R. M. Fulrath, J. Am. Ceram. Soc. **46**, 146 (1963).
7. D. L. Branson, J. Am. Ceram. Soc. **48**, 591 (1965).
8. El-H. M. Diefallah, A. O. Baghlaf, M. S. El-Meligy, and E. A. Abu El-Futooh, Radiat. Phys. Chem. **27**, 123 (1986).
9. A. A. El-Bellihi, A. M. Abdel-Badei, and El-H. M. Diefallah, Thermochim. Acta **165**, 147 (1990).
10. W. W. Wendlandt, "Thermal Methods of Analysis." Wiley–Interscience, New York, 1964.
11. M. E. Brown, "Introduction to Thermal Analysis," Chap. 13. Chapman and Hall, London/New York, 1988.
12. E. Pincovschi, I. Maxim, and T. Ionescu, Z. Anorg. Allgem. Chem. **356**, 207 (1968).
13. J. G. Dunn and L. C. Mackey, J. Thermal Anal. **37**, 2143 (1991).
14. A. K. Galwey, "Thermal Analysis." (B. Miller, Ed.), Vol. 1, p. 38. Wiley, New York, 1982.
15. El-H. M. Diefallah, Thermochim. Acta **202**, 1 (1992).